PINSA, **64, A**, No 3, May 1998, pp. 365-375.

RECENT ADVANCES ON EQUATORIAL SPREAD F

P B RAO AND A K PATRA

National MST Radar Facility, P O Box 123, Tirupati 517 502, India

(Received 04 December 1997; Accepted 29 January 1998)

Equatorial spread F (ESF), a manifestation of the plasma instabilities in the F region of the equatorial ionosphere, has been a subject of active study for well over five decades. The early phase of ESF studies, based mainly on ionosonde data, was concerned primarily with the morphological description and statistical characterization of the phenomenon. The application of high power VHF/UHF radar, rocket and satellite techniques, coupled with theoretical and numerical simulation studies, marked the beginning of a new phase of studies providing a physical insight into the plasma instability processes governing the onset and evolution of the ESF. The experimental and theoretical developments in the field having been covered in earlier reviews, for the most part, the scope of this paper is limited to an overview on the recent advances on ESF of current interest. The aspects dealt with, in particular, are : effects of vertical wind and electric field on the evolution of ESF, gravity wave seeding of ESF, updrafting and downdrafting of plasma bubbles associated with ESF, and the role of steepened structures and drift waves in the development of ESF.

Key Words : Ionosphere; Equatorial Spread F; Plasma Instabilities.

1. Introduction

The equatorial spread F (ESF) has been studied quite intensively ever since it was first observed as characteristic spread or diffuse condition of the F-region returned echo on the ionogram[1]. The ESF, although meant originally to convey spread condition of the ionogram trace, it has now become generic to mean a wide class of irregularities in the F region with scale sizes ranging from a few hundred kilometers to a few centimeters. The early phase of ESF studies, based primarily on ionosonde data, was concerned mostly with the statistical and morphological aspects of the phenomenon and has been reviewed in detail by Herman[2]. The entering of the high power radars on to the scene as a powerful means to map the structure and dynamics of ESF irregularities[3,4], combined with the *in situ* observations by rocket and satellite techniques[5,6], marked the beginning of a new phase of the ESF studies. In parallel to the observations by the advanced experimental techniques, there have been rapid advances in theoretical and numerical simulation studies of the ESF[7,8,9,10,11]. The combined efforts of experimental and theoretical studies have contributed greatly to the current insight into plasma instability processes driving the ESF irregularities. The experimental and theoretical developments, starting from the early radar observations and simulation studies, have been, for the most part, extensively reviewed in a number of papers[12,13,14,15]. Hence, the scope of this paper is confined to an overview on only the recent advances on some of the important aspects of the ESF of current interest. The specific aspects that are dealt with include : 1) the influence of the background electric field and neutral wind on the nonlinear evolution of the ESF, 2) the role of gravity waves on the generation of the ESF, 3) updrafting and downdrafting of the plasma bubbles (plasma depleted magnetic flux tubes) and 4) the role of steepened structures and drift waves.

The ESF, according to the current view, is initiated in the post sunset bottomside F-region at longer wavelengths through a collisional Rayleigh-Taylor (RT) instability and extended to shorter wavelengths through secondary processes[13]. The evolution of the ESF has been studied extensively by means of nonlinear numerical simulation studies of the RT process. The recent simulation studies by Sekar *et al*[16]. take into account the effects of vertical winds and zonal electric fields on the nonlinear evolution of the ESF. It was shown through simulation that a downward wind of $20ms^{-1}$ would accelerate the evolutionary process of ESF with significant effects extending even beyond 350km. The effects of same magnitude could be realized by introducing an eastward electric field of $0.76mVm^{-1}$ instead of vertical wind. It was suggested that the day-to-day variability of vertical winds could be responsible for the day-to-day variability in the evolutionary characteristics of the ESF. This aspect of the nonlinear simulation study of the ESF is described in some detail in section 2.

In the evolution of the ESF, one of the important factors is the seed perturbation which is believed to be provided by internal atmospheric gravity waves[17,18,19]. The gravity waves as a source of the seed perturbation for the evolution of RT process are particularly effective under conditions of spatial resonance[20]. It was shown recently by

Sekar *et al*[21] that a seed perturbation as small as 0.5% could evolve into ESF provided the nonlinear effects of the vertical wind and electric field are taken into account. Huang and Kelley[22] have carried out recently a simulation study of the nonlinear evolution of the ESF using a large scale gravity wave seeding and smaller-scale initial density perturbation. They have shown through the simulations that the large-scale gravity wave determines the outer scale of the ESF irregularities by seeding the RT instability and the smaller scale perturbation results in multiple plumes on the west wall of a plasma upwelling. In a recent study, Prakash[23] has proposed a new mechanism for the seed perturbation in the base of the F-region that is large enough to initiate the ESF. The mechanism involves the generation of electric field perturbations by gravity wave winds in the E-region and their coupling to the F-region along the field lines. Using realistic model parameters, it was shown that it is possible to generate an electron density perturbation in excess of 5% that is normally adopted in the simulation of the ESF. These recent developments on the role of gravity waves as seed perturbations in the evolution of ESF are discussed in section 3.

The numerical simulation studies carried out on the collisional RT instability process have shown that in the nonlinear regime, the instability development would lead to the generation of plasma bubbles (plasma depleted magnetic flux tubes) in the bottomside and their evolution into the topside[10,11,13]. There have been a number of theoretical studies aimed at understanding the vertical motion of the plasma bubbles associated with the ESF[24,25,26,27]. Using San Marco D satellite data, Laakso *et al*.[28] were the first to report an updraft followed by a downdraft of the plasma bubbles. Recently, using the high power VHF radar at Gadanki, Rao *et al*[29]. have shown that downdrafting plasma flow in a depletion channel extends as high as 550km in the topside and down all the way to E-region in the bottomside. The theoretical and experimental studies on the updrafting and downdrafting aspects of the plasma bubbles associated with the ESF are presented in section 4.

In the context of the nonlinear evolution of the ESF, the possibility of plasma organized in steepened structures leading to drift waves was first addressed by Costa and Kelley[30]. According to the model proposed by them, a long wavelength RT mode nonlinearly evolves into steepened structures having power spectra varying as k^{-2}. The steep gradients are unstable to drift waves which may be responsible for some of the VHF radar observations associated with the ESF. In a recent study based on simultaneous rocket and radar observations at Kwajalein and related modelling by Hysell *et al*.[31,32,33], it was shown that the ESF is characterized by steepened structures, and the coherent echoes observed at 50MHz by the Cornell University portable radar interferometer and Jicamarca radar are due mainly to backscatter from these structures. A discussion on the role of steepened structures and drift waves as brought out in the above studies is presented in section 5.

Some special features which include bifurcation of plasma bubbles, valley region ESF, explosive ESF and supersonic velocities of the plasma bubbles form the content of section 6.

2. The Evolution of ESF

The high power radar observations made by Woodman and LaHoz[3] at Jicamarca marked the beginning of a new phase in the study of ESF. The plumes observed on the radar Range-Time-Intensity (RTI) maps have been interpreted in terms of plasma bubbles generated in the post-sunset bottomside F-region and extended into topside due to buoyancy. The authors postulated the existence of large bubbles produced by nonlinear development of the gravitational Rayleigh-Taylor (RT) instability. That the plumes in the RTI maps do indeed represent plasma bubbles has been confirmed through overwhelming evidence from combinations of radar, rocket and satellite observations[4,5,6,17,34]. Simultaneous topside radar backscatter maps and *in situ* rocket measurements were made during the PLUMEX-1 rocket flight[5,34]. The most intensive backscatter was found to be co-located with the plasma density depletion[5]. The plume like feature in the radar map is tilted to the west and extends well into the topside. Further evidence for the essential validity of the bubble concept has come through nearly simultaneous incoherent and coherent backscatter measurements with the Altair radar at Kwajalein. The Altair radar has also been used to scan in the north-south direction to study the field aligned nature of the structures. The VHF radar observations at Jicamarca and VHF and UHF at Kwajalein have shown evidence of small scale irregularities at 3, 1.93, 0.36 and 0.11m during ESF[35,36,37].

An important breakthrough in understanding ESF came through the first numerical simulation of the Rayleigh-Taylor instability by Scannapieco and Ossakow[10]. Their simulation shows the production of plasma bubbles in the bottomside F-region and their extension to the topside through nonlinear evolution. Further simulations considered the dependence on altitude of the F-peak, density gradient scale length[38], initial perturbations of varying horizontal scale length, neutral wind and background Pedersen conductivity[11,39]. The simulations show a remarkable agreement with the radar observations of equatorial spread F.

In the recent years, extensive experimental, theoretical and numerical simulation studies have been performed on various aspects of the ESF[20,21,22,28,29,31,32,33,40,41,42,43]. The Kwajalein observations made with the Cornell University Portable Radar Interferometer (CUPRI) system (Hysell *et al*.[33]) show many periodic plume structures with no bottomside band structures unlike at Jicamarca. The most recent observations on the evolution of the ESF are

from the recently established MST radar at Gadanki, India. Figs. 1a & b show the power maps observed at Gadanki on March 29 and September 30, 1994. The power map observed on March 29 shows a bottomside band structure followed by two discrete near vertical plume structures resembling closely the plasma bubbles simulated through nonlinear RT process[11,16]. Following the occurrence of the plumes, the bottomside slab structure, which is intact, is found to descend at a rate of about 70ms^{-1} all the way to the E-region, an unsual feature observed at Gadanki. The observations of September 30 also show similar downdrafting feature but the structures are much different from that observed on 29 March. The observations also show many periodic plume structures in contrast to that observed over Jicamarca and somewhat similar to that observed over Kwajalein[29]. From the observations it is clear that while the basic instability mechanism for the generation of the large scale structures is established, there are still some aspects which need to be understood further.

In order to understand the various features of the ESF structures, a number of studies have been performed in the recent years taking various destabilizing agencies into account with the basic mechanism as RT process. The effect of zonal electric field and the zonal wind with tilted ionosphere to enhance or inhibit the growth of the RT mode has been included in the so called Generalized Rayleigh-Taylor (GRT) instability[43]. In such a case, the linear growth rate applicable to the equatorial geometry may be written as

$$\gamma_{RT} = \frac{E_{x0}}{LB} + \frac{g}{\nu_{in}} \cos\sigma + \frac{E_{z0}+ uB}{LB} \sin\sigma, \qquad ...(1)$$

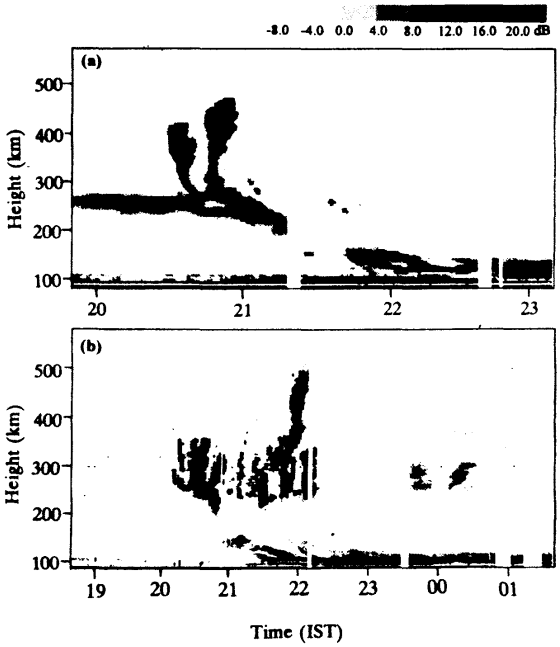

Fig 1 Height-time-intensity maps of the backscattered signal from spread F irregularities observed at Gadanki on *(a)* 29 March 1994 (after Patra *et al*[42].) and *(b)* 30 September 1994 (after Rao *et al.*[29]).

where L is the gradient scale length on the bottomside, σ is the tilt angle, which is measured positive from east toward the zenith, the z axis is upward and the x axis is eastward.

Raghavarao *et al.*[44] have studied the effect of vertical winds on the growth rate of the RT instability. The growth rates for the GRT instability with different destabilizing factors computed by them are shown in Fig. 2. They have shown that a downward wind of 1ms^{-1} can cause the same growth rate as a 200ms^{-1} eastward wind at 260km, while a 16ms^{-1} downward wind at 300km can be as effective as that of gravitational drift. Recently, Sekar *et al.*[16] examined the effects of vertical winds and electric fields on ESF and indicated that the downward vertical wind and eastward electric field accelerate the evolutionary process of ESF. Their investigation is based on a two dimensional non-linear simulation model with a slab geometry of the ionosphere. The x, y and z axes are directed westward, upward and northward respectively. They have used the equations of ion and electron momentum, continuity and current conservation as the basis for their simulation. Under certain valid assumptions, these equations are reduced to two differential equations :

$$\nabla.(\nu_{in} n \nabla \varphi_1) = -\frac{B}{c} g \frac{\partial n}{\partial x} + \frac{B}{c} W_y \nu_{in} \frac{\partial n}{\partial x} + \nu_{in} E_x \frac{\partial n}{\partial x} \qquad ...(2)$$

and

$$\frac{\partial n}{\partial t} - \frac{\partial}{\partial x}\left(\frac{nc}{B}\frac{\partial \varphi_1}{\partial y}\right) + \frac{\partial}{\partial y}\left(\frac{nc}{B}\frac{\partial \varphi_1}{\partial x}\right) = -\nu_R n. \qquad ...(3)$$

Eq. (2) is the differential equation for the perturbation potential (φ_1) in a generalized form, wherein the effects of vertical winds (W_y) and zonal electric field (E_x) are included apart from the RT term due to gravity (g). Eq. (3) represents the plasma continuity equation wherein the dominant transport term and the recombination effects are included, the production being assumed to be zero. Using a sinusoidal perturbation of 5% amplitude and suitable boundary conditions for both the perturbation potential and the plasma density in zonal direction, the differential equations are solved numerically. The model calculations are performed using (1) gravity alone as the driving agency and (2) vertically downward wind of magnitude 20ms^{-1} along with gravity as the driving agency. The result of this simulation is shown in Fig. 3. It is shown that the effect of 20ms^{-1} vertical wind is equivalent to the effect of eastward electric field of 0.76mVm^{-1}. They have concluded that the effects of vertical winds and eastward electric fields are significant even beyond 350km where they are considered to be less important according to linear theory.

In a further nonlinear simulation, Sekar *et al.*[21] have shown that even an order of magnitude less perturbation (0.5%) than that used earlier (5%) grows into a bubble

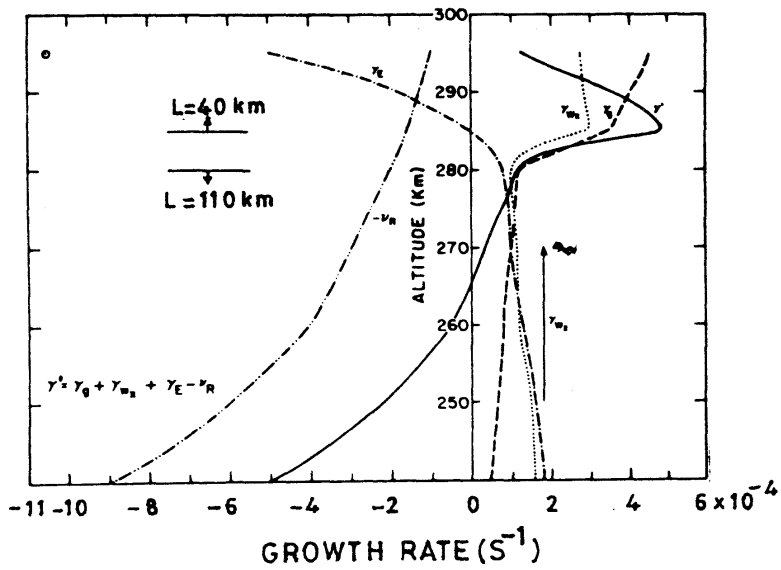

Fig 2 Computed growth rates for the destabilizing factors, viz., gravity, electric field, eastward wind for a tilted ionosphere (10°) and vertical wind for two regions of plasma scale lengths L (110km and 40km). γ' is the algebraic sum of these growth rates, with the effective recombination coefficient (ν_R) also depicted (after Raghavarao *et al*[44]).

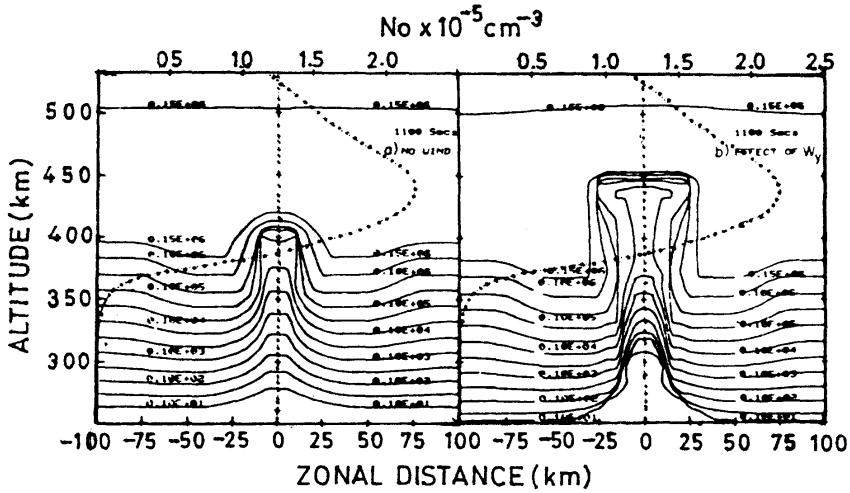

Fig 3 Isoelectron density contours in zonal and vertical plane at 1100 sec after the onset time of the instability for the cases *(a)* effects of gravity alone and *(b)* with a downward wind of 20ms^{-1} along with gravity (after Sekar *et al.*[16]).

provided the nonlinear effects of either agency such as the vertical wind and the electric field, in addition to gravity, are taken into account. Such a small perturbation in plasma density can be generated by the fluctuating electric field which is often present in the evening ionosphere.

Sekar and Raghavarao[45], in a separate simulation have shown that the plasma density distribution on the topside of the equatorial ionosphere plays a dominant role in the plasma bubble characteristics, viz., horizontal width, vertical extent and its dynamical behaviour. The differences in the widths and shapes of the plasma bubbles/plumes observed over Kwajalein and Jicamarca have been attri-buted to the differences in the plasma density distribution in the topside ionosphere at the two locations.

3. Role of Gravity Waves on the Generation of ESF

A long standing problem concerned with the ESF is in relation to the seeding mechanism which can help accelerate the otherwise relatively slow growth of the RT instability. Studies dating back more than 2 decades have

presented evidence that atmospheric gravity waves play a significant role in initiating nighttime equatorial F-region instability. Rottger[46,47,48] reported a series of wavelike structures of large-scale ESF irregularities and put forward the notion that the gravity waves produce these structures *via* the spatial resonance mechanism. Klostermeyer[49] performed the numerical calculations of the spatial resonance mechanism using a turbulent dissipation to limit their amplitude and applied his results to explain the observations of Rottger[46,47,48]. However, Kelley *et al.*[17] argued that gravity wave interaction alone cannot yield a large displacement observed without further amplification by the RT instability. The observations of Kelley *et al.*[17] and more recently that of Hysell *et al.*[33] and Rao *et al.*[29] show such periodic structures which correspond to medium scale gravity waves. It has, therefore, become a common practice to invoke the gravity wave as the seed perturbation for the growth of the RT instability. A RTI map observed recently at Kwajalein[33], revealing many periodic plume structures, is shown in Fig. 4. There are as many 10 plumes which are separated in time by 20-30min. Huang *et al.*[19] have proposed a theory of gravity wave seeding of ESF. They have shown analytically that gravity waves can initiate the RT instability and result in large amplitude ionospheric perturbations when the drift velocity of plasma is equal to the phase velocity of the seed gravity wave which is termed the spatial resonance. In a recent two-dimensional simulation, Huang and Kelley[22] have reproduced the periodic plume structures as shown in Fig. 5. When a large-scale seed gravity wave and a small-scale initial density perturbation are used simultaneously, it is observed that the large-scale gravity wave determines the outer scale of the ESF irregularities by seeding the RT instability and the small scale perturbation results in multiple plumes preferentially located on the west wall. They have also reproduced the bifurcation of plasma bubbles in their simulation.

A new mechanism for the generation of the ESF by the E-region perturbation electric field has been proposed by Prakash and Pandey[50]. They have examined the possibility of the perturbation electric field associated with the E-region irregularities as the seed for the ESF generation. The perturbations in electric field, when transmitted to the F-region, can generate the electron density structure required for the seed perturbation to initiate the ESF. They have assumed the gravity wave wind driven electron density irregularity as the mechanism for the perturbation electric field in the E-region. Perturbations in electron density of gravity wave scales have been measured in the E-region over Sriharikota. In a recent study, Prakash[23] has proposed a new mechanism for a seed perturbation in the base of the F-region that is large enough to initiate the ESF. According to this mechanism, the zonal winds in the intermediate region and the F-region give rise to the radial electric fields which together with zonal fields drive currents in the E-region where the flux tube integrated Pedersen and Hall conductivities are perturbed by the electron density irregularities produced by gravity wave wind. This results in the perturbations of zonal and radial electric fields which, in turn, produce seed irregularities in the base of the F-region. Using realistic values of various parameters, the amplitude of perturbations in the vertical plasma drift velocities have been found to be $6.5 ms^{-1}$. This amplitude is sufficient enough to produce 5% perturbation in electron density near the base of the F-region normally used in the simulation of the ESF.

4. Updrafting and Downdrafting of Plasma Bubbles

The dynamics of the plasma bubbles (plasma depleted magnetic flux tubes) is one of the important aspects of the phenomenon of equatorial spread F (ESF). There have been a number of studies aimed at understanding the vertical motion of the plasma bubbles associated with the ESF[24,25,26,27]. The theoretical model of Ott[24] showed that in the collisional limit of the RT process, the bubble rise velocity depends on its altitude through the ion-neutral collision frequency, but not on its size. In the inertial limit, however, the velocity is independent of altitude but depends on the bubble size with velocity proportional to the square root of the radius of the rising bubble in a fluid. Ossakow and Chaturvedi[25] have analyzed the rise velocities of the plasma bubbles in the collisional RT regime for different bubble shapes. The analysis has made evident the implication of zonal electric field to the bubble rise velocity for the case of a linear model. They have pointed out the effect of nighttime westward electric field on the vertical motion of the plasma bubbles but made no mention about the downward motion of the plasma in the depletion channel. Further insight into the vertical motion of plasma bubbles has been gained through the work of Anderson and Haerendel[27] who considered the problem, incorporating flux tube integrated quantities of electron content and Pedersen conductivity. According to them, if the ambient electric field reverses direction during the bubble's initial growth phase, the depleted region will change direction and move downward but not necessarily with the velocity greater than the ambient plasma drift.

The discussion related to the plasma bubbles associated with the ESF, however, was concerned generally with the rising bubbles or plumes as seen from both theory and observations. Laakso *et al.*[28] were the first to report an updraft followed by a downdraft of the plasma bubbles from the San Marco D equatorial ionospheric satellite data. Fig. 6 shows the simultaneous observations of depletion and the westward electric field. The westward electric field is observed as high as $4 mVm^{-1}$ which means the plasma in the depletion region is moving downward with $\sim 160 ms^{-1}$. They have shown that both updrafting and downdrafting can be expected on the basis of the RT

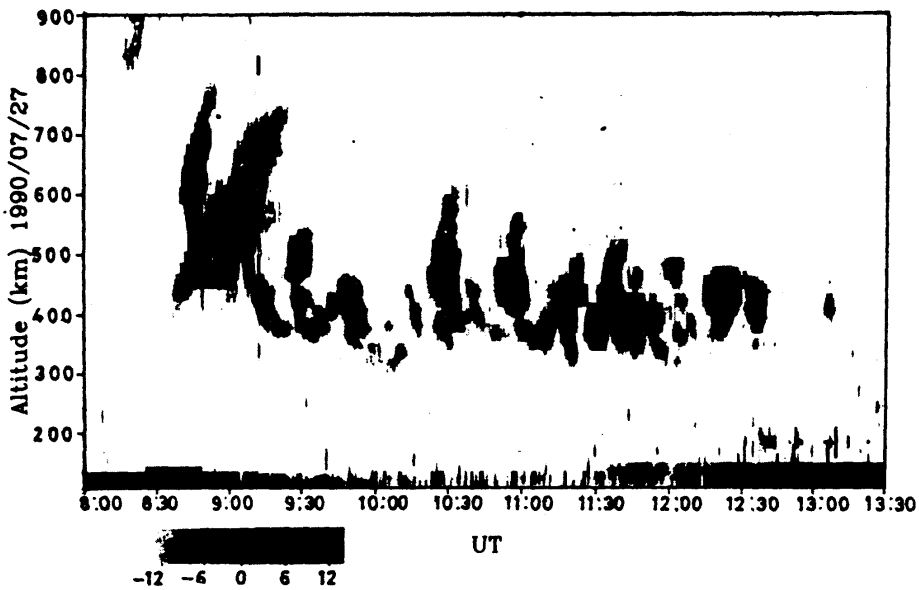

Fig 4 Coherent backscatter power received by the CUPRI radar on 27 July 1990 as a function of range and time (RTI) (after Hysell *et al.*[33]).

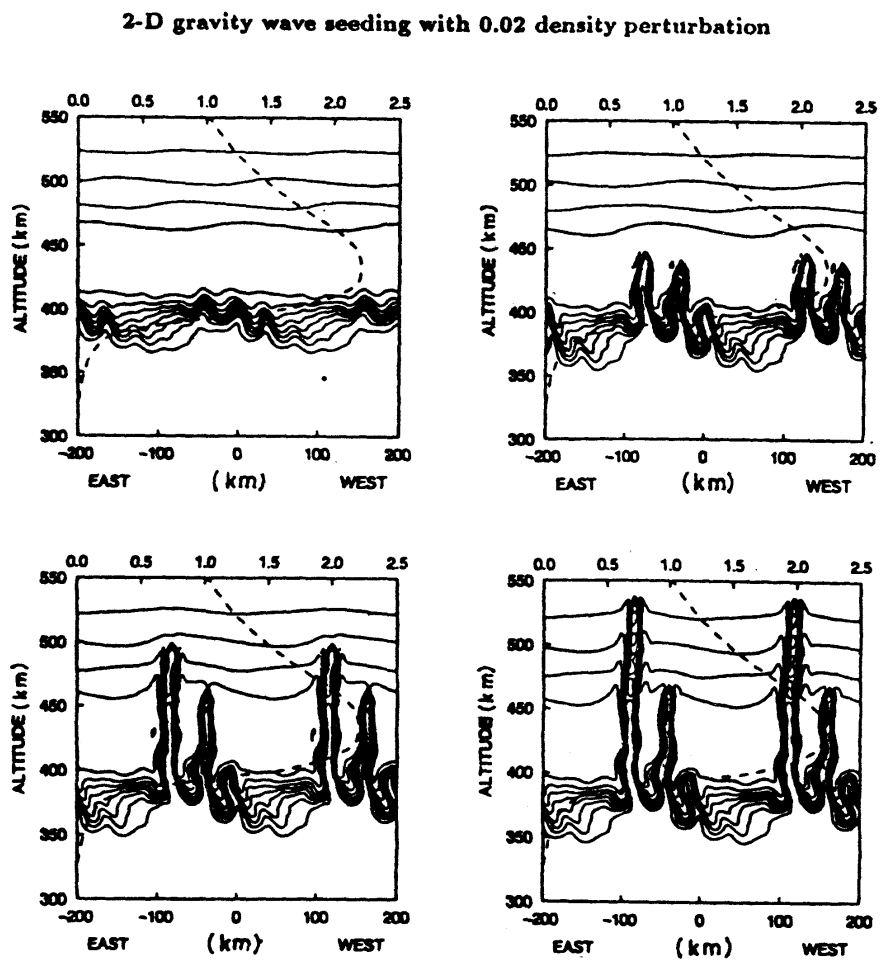

Fig 5 Isodensity contours for two-dimensional gravity wave seeding with 2% density perturbation at smaller scale. The horizontal and the vertical wavelengths of the smaller-scale density perturbation are 33 and 15km respectively (after Huang and Kelley[22]).

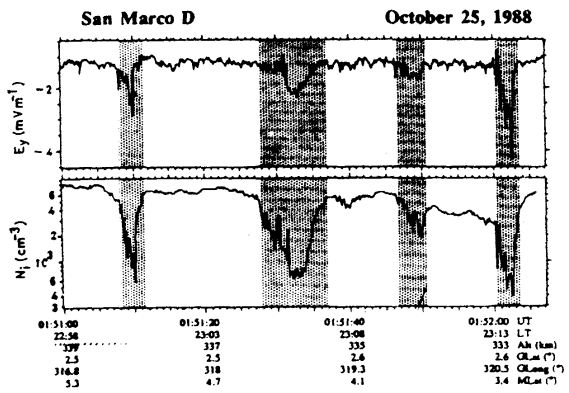

Fig 6 Density depletion regions crossed by San Marco D on 15 October 1988, 0151.00-0152.10 UT. The upper panel is the y-component of the d.c. electric field (E_y) and the bottom panel is the ion density (N_i). Density depletion regions shaded in gray are associated with enhanced zonal electric fields resulting in large vertical plasma flows (after Laakso *et al.*[28]).

instability process. They have calculated the electric field inside the bubble using the basic equation of momentum applicable to charged particles. This includes four driving forces that affect the motion of the charged particles in the F-region: electric field, neutral wind, gravitation and pressure gradients. Neglecting the pressure gradient term (being small), they have expressed the irregularity vertical drift velocity as:

$$V_{x1} = \frac{E_{y0}}{B} + \left[\frac{g}{\nu_{in}} - U_x + \frac{E_{y0}}{B}\right]\left[\frac{n_0}{n_1} - 1\right], \qquad \ldots (4)$$

where E_{y0} and n_0 are the background eastward electric field and the electron density, n_1 the electron density inside the depletion, g the gravity, ν_{in} the collision frequency and U_x the vertical neutral wind. From the above expression they showed that as the background zonal electric field becomes westward, the plasma in a depletion channel may assume a downdrafting motion at altitudes less than about 400km, while the flow remains upward at higher altitudes. Such a simultaneous occurrence of the updrafting and downdrafting plasma flow in a single bubble channel may lead to the pinching off of the upper part of the depletion region from the lower part.

On the plasma flow inside the depletion channel, the most recent VHF radar observations by Rao *et al.*[29] have brought out some interesting new features. These observations were made with two VHF radars, one at Gadanki (mag. lat. 6.3°N) and the other at Trivandrum (mag. lat. 0.3°N). The observations have shown that plasma inside a bubble can assume both upward and downward drifts depending upon the background zonal electric field and the vertical neutral wind. They have observed downward motion extending to as high as 550km in contrast to the model prediction given by Laakso *et al.*[28]. Figs. 7*a*&*b* show respectively the Height-Time-Intensity (HTI) and velocity maps observed on 1 March 1996, representing the vertical irregularity drifts associated with the ESF. It should be pointed out that the observations made by Laakso *et al.* are limited in the sense that the satellite measures only at a particular height whereas the radar provides the drift of the irregularities over a large extent of altitude. To explain the downdrafting extending upto 550km in their observations, they have emphasized the importance of the field-line integrated plasma parameters instead of the local parameters in contrast to that of Laakso *et al.*[28].

The simultaneous radar observations made at Trivandrum and Gadanki on 21 March 1995 are shown in the form of HTI maps in Fig. 8. The observations, with two prominent structures during 2050-2210hrs, are found to be well correlated and, normalizing to the same system sensitivity, the peak signal intensity at Trivandrum is about 6dB above that at Gadanki. The height levels of the maximum signal intensity associated with the two plasma upwellings at Gadanki and Trivandrum are found to be about 325 and 400km. This height difference is in good agreement with the difference of 80km in the height of the magnetic flux tube linking Gadanki to the equator at the height of 400km. For the radar geometry at Trivandrum, using the observations of maximum range extent and the time it takes for a depletion channel to drift through the radar beam, it is possible to infer the zonal dimension and drift velocity of the depletion channel. For the observed two depletion channels, they are estimated to be 70km and 70ms^{-1} and 90km and 70ms^{-1}. The estimates of zonal dimension obtained here are of the same order as reported from the satellite observations[28].

The height-time variations of the Doppler velocity observed on 21 March 1995 at Trivandrum and Gadanki are presented in Fig. 9. The velocities observed at Gadanki are found to be in the range of about 100 to -50 ms^{-1}. For Trivandrum, where the radar is directed at 30° magnetic west of zenith, the velocities fall in the range of about 50 to −120ms^{-1}. The velocities are found to be predominantly negative which seems to be due to an eastward flow of plasma during nighttime. For a zonal drift of 70ms^{-1} as inferred from the HTI maps, the vertical velocities for the two dominant structures are estimated to be downward at 40 and 75ms^{-1} as against 30 and 50ms^{-1} at Gadanki. These values are well above the nighttime downward background plasma drift velocity implying that the downdrafting structures are plasma depletions.

5. Steepened Structures and Drift Waves

An analytical model by Chaturvedi and Ossakow[51] for the bottomside ESF indicates a coherent development of the RT instability which is likely to evolve into steepened structures. The role of steepened structures and drift waves

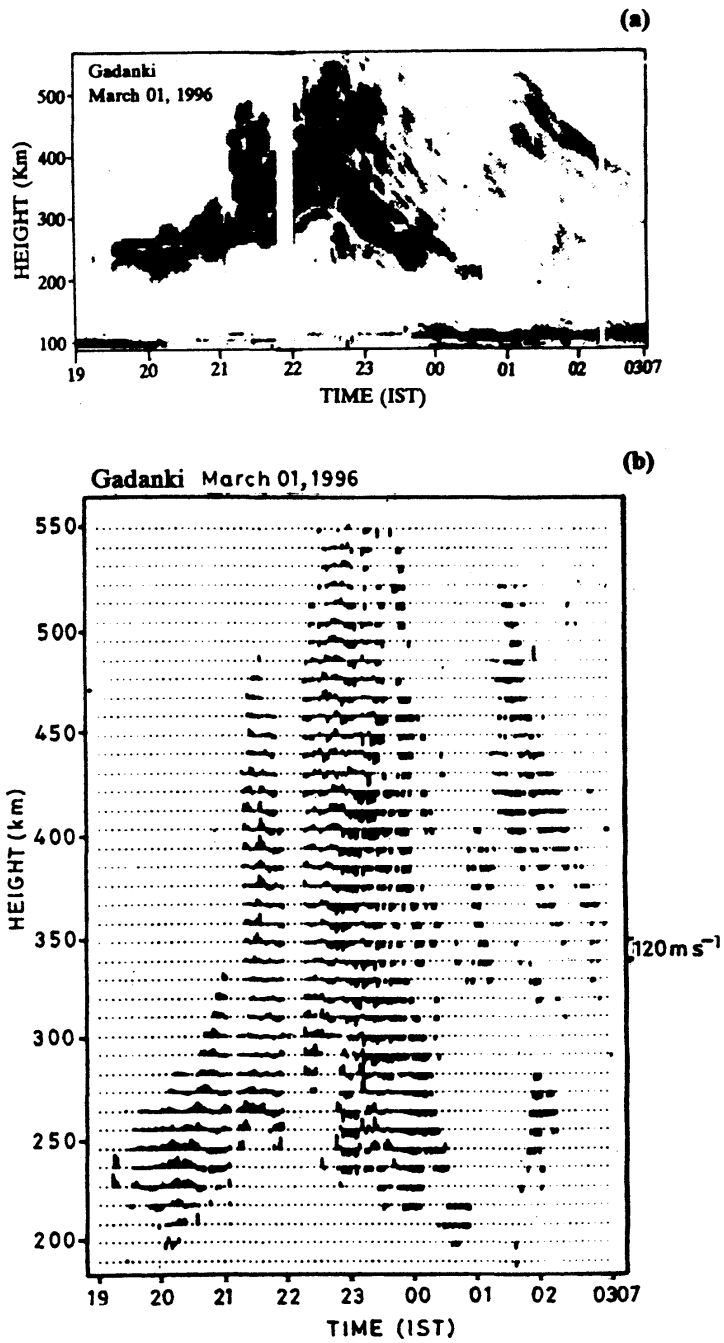

Fig 7 *(a)* Height-time-intensity maps of the backscattered signal from spread F irregularities; and *(b)* associated Doppler velocities observed at Gadanki on 01 March 1996 (after Rao *et al.*[29]).

in the context of the nonlinear evolution of the ESF has been examined by Costa and Kelley[52]. According to the model proposed by them, a long wavelength RT mode nonlinearly evolves into steepened structures having power spectra varying as k^{-2}. The steep density gradients are unstable to short-wavelength drift waves which evolve from the nonlinear development of an unstable long-wavelength mode. A linear theory for the collisionless drift wave instability given by Costa and Kelly[52] shows that the growth rate is maximum for $k_i \rho_i \approx 1.5$, where k_i is the wavenumber of the drift wave and ρ_i is the ion gyroradius. Huba and Ossakow[53] have given a linear theory for low-frequency collisional drift waves and showed that the drift waves in the 3 meter regime, which are of interest to the VHF radar observations at Jicamarca, are heavily damped due to ion viscosity. It was shown that, unless $n < 2 \times 10^3$

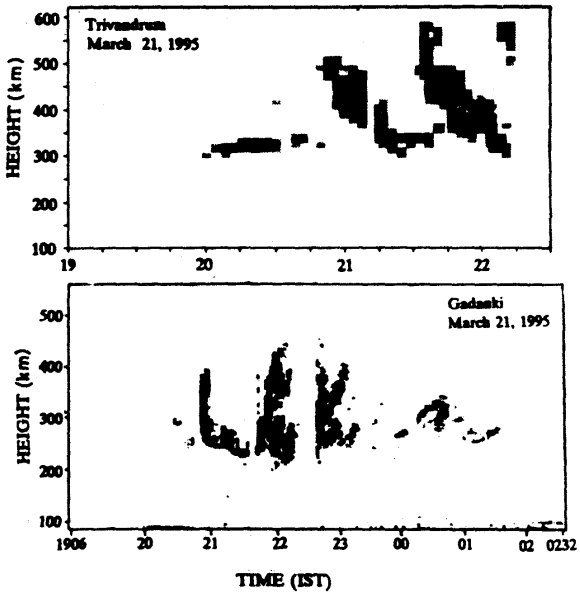

Fig 8 Height-time-intensity maps of the backscattered signal from spread F irregularities observed on 21 March 1995 at Trivandrum (top) and Gadanki (bottom). (after Rao *et al.*[29])

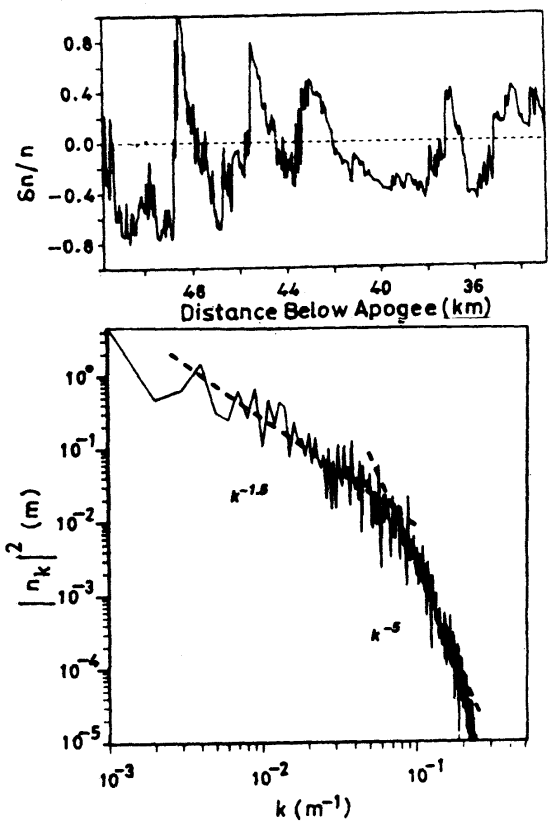

Fig 10 Detrended perturbation electron density profile extracted from the downleg of rocket flight 29.028. The horizontal scale is the distance below apogee in kilometers (top). The average power spectral density constructed from the spectra of four sequential simulated density profiles (bottom) (after Hysell *et al.*[32]).

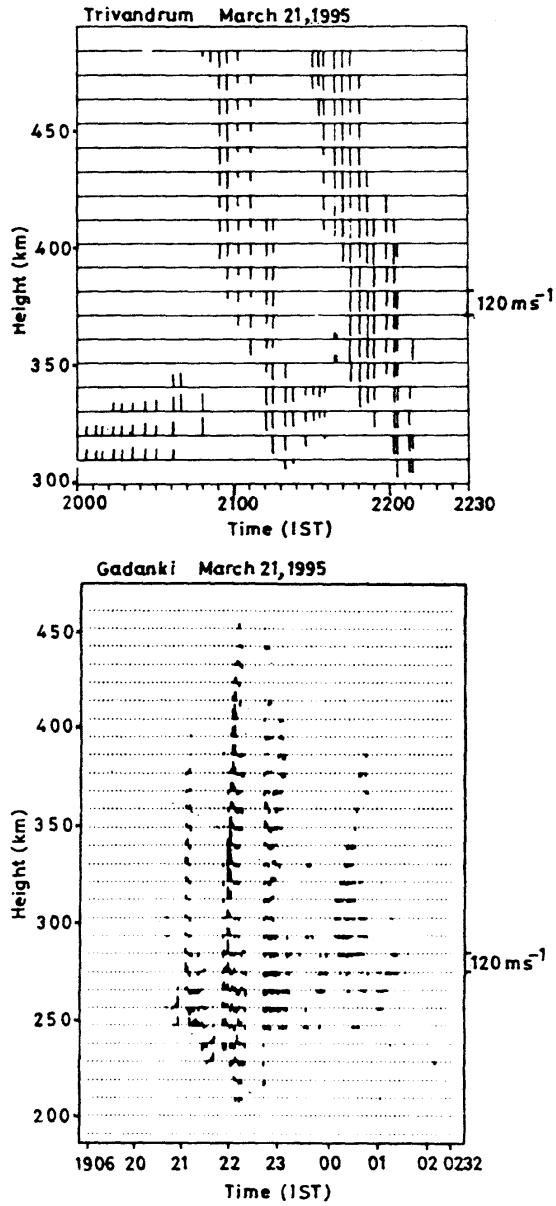

Fig 9 Height-time variation of the Doppler velocity of the irregularities observed in the direction 30° due magnetic west of zenith at Trivandrum (top) and transverse to the magnetic field in the meridian plane at Gadanki (bottom) (after Rao *et al.*[29])

cm^{-3} for density gradient scale lengths of $\gtrsim$75m, it is improbable that low frequency drift waves can linearly generate the 3m irregularities observed during ESF. Using rocket data of project Condor, LaBelle *et al.*[54] have confirmed that at altitudes above 280km, the spectrum of density irregularities follows $k^{-2.5}$ for larger scale sizes (λ <100m) and k^{-5} for shorter scale sizes (λ < 100m). They have found that, while the low altitude spectrum is consistent with classical electron diffusion, the high altitude spectrum requires a diffusion coefficient enhanced by 2-3 orders of magnitude above classical diffusion. The en-

hanced diffusion coefficient is consistent with the anomalous diffusion that could arise from drift waves as a result of nonambipolar diffusion and wave-particle interaction acting at the scale of ion gyroradius.

The role of steepened structures has been further examined by Hysell *et al.*[32] using data from simultaneous radar and rocket experiments at Kwajalein during July-August 1990. The rocket experiments have shown that the unstable nighttime F-region is characterized by propagating steepened structures. A plot of $\delta n/n$ with distance showing steepened structures and its power density spectrum are shown in Fig.10. The power spectra exhibit two regions that obey k^{-n} scaling, where n is in the range of 1.5 to 2 at wavelengths greater than 80-100m and 4.5 to 5 at shorter wavelengths. Hysell *et al.*[33] have developed a semiemperical model of the three-dimensional spectrum of the ESF irregularities that is consistent with the one-dimensional spectra of density fluctuations observed by the sounding rockets. The radar cross-section at 3m computed from the model is found to be with in a dB of that measured by the Cornell University Portable Radar Interferometer (CUPRI). It was argued that the coherent echoes measured by CUPRI and Jicamarca radar are due mainly to scatter from the steepened structures, and the Doppler spread of the echoes is due to the advection of the structures. The possibility of drift waves contributing to the other scattering modes, however, is not entirely ruled out.

6. Special Features

a) Bifurcation of Plasma Bubbles

Bifurcation of plasma bubbles as they evolve into the topside is a feature that has been observed in both radar and airglow measurements[3,54]. Recently, the bifurcation phenomenon has also been observed *in situ* with the San Marco D satellite data by Aggson *et al.*[55]. Two possible ways have been advanced to explain the bifurcation phenomenon: (1) If a stream of plasma flow is significantly wide, it would bifurcate due to differential motion. This differential motion is due to the localized vertical polarization electric fields at different locations within the bubble. For this case to occur, we have to have a large bubble in the zonal direction. (2) If a stream encounters an obstruction, it could lead to the bifurcation of the bubble and this could happen to both large and narrow bubbles. If the top of the bubble (the outer boundary of the depleted flux tube) encounters a highly conducting E-region (e.g., sporadic E) at the foot of the flux tube, it could give rise to bifurcation. In this case the conducting E-region can be considered as an obstacle[39]. Recent numerical simulations reported by Huang and Kelley[21,22,49] show clearly the bifurcation of the plasma bubbles. Their simulations suggest that the bifurcation process is a highly nonlinear process. It appears now that although the bifurcation is seen both in observations and simulations, the process at work is far from understood and needs further study.

b) Valley Region Irregularities

The valley region irregularities which occur inbetween the E and F regions of the ionosphere during nighttime are evident from the radar observations[3,29,41,42]. The valley region irregularities observed at Jicamarca are often associated with the rising plasma bubbles. From these observations, Woodman and LaHoz[3] and Woodman[56] have invoked the polarization electric field associated with the bubble as the source for these irregularities. The east-west electric field associated with the bubble sucks the plasma from the E-region probably generated through the meteoric ionization. Recently, Sekar *et al.*[57] have modelled the effect of the fringe field associated with the F-region irregularities on the low altitude plasma. They have found that the fringe field could generate the valley region irregularities. While some of the valley region irregularities can be explained using the above mentioned mechanism, the valley region irregularities observed at Gadanki[29,42] cannot be explained following the above mechanism. Often the valley region irregularities observed at Gadanki are found to descend all the way from F-region to the E-region which could not be explained by the fringe field effect. Hence, it appears that although a plausible mechanism has been proposed, it does not seem to account all the features that are observed in the valley region associated with the ESF.

c) Explosive Spread F

The explosive spread F as reported by Woodman and LaHoz[3] is a phenomenon associated with the ESF with lifetime as short as few hundreds of milliseconds and is not a common feature. Since then, the only observations which appear to be similar in nature are that reported by Hysell and Farley[41]. The short life time of the instability seems to be the most important factor to make the measurements of this phenomenon hard with a radar. Very high time resolution observations could do the needful but such attempts are rare. No mechanism has yet been advanced to account for the explosive ESF. Further observations are essential to understand the basic characteristics of the phenomenon and to arrive at a possible mechanism.

d) Supersonic Plasma Flow Associated with ESF

Although supersonic plasma flow in the ionosphere was predicted by Chandrasekhar[58], it was not possible to measure it until the development of modern measurement techniques. Supersonic plasma flow in a plasma depletion has been observed *in situ* using the San Marco D satellite

data[40]. Radar observations[33] have also shown the supersonic velocities associated with the topside ESF. The observed velocities are as high as 1200ms^{-1} which correspond to a polarization electric field of about 40mVm^{-1}.

7. Acknowledgements

Authors are grateful to Dr B V Krishna Murthy of SPL, VSSC, Trivandrum for having gone through the manuscript and offered suggestions for its improvement. One of the authors(AKP) would like to thank NMRF for Visiting Research Fellowship and UGC-SVU Centre for MST Radar Applications for the support during the preparation of this paper. The National MST Radar Facility (NMRF) is operated as an autonomous facility under DOS with partial support from CSIR.

8. References

1 H G Booker and H W Wells *Terr Magn atmos Elect* **43** (1938) 249
2 J R Herman *Rev Geophys* **4** (1966) 255
3 R F Woodman and C LaHoz *Geophys Res* **81** (1976) 5447
4 R T Tsunoda *J atmos Terr Phys* **42** (1980) 743
5 C L Rino, R T Tsunoda, J Petricks, R C Livingston, M C Kelley and K D Baker *J. Geophys Res* **86** (1981) 2411
6 R T Tsunoda, R C Livingston, J P McClure and W B Hanson *J Geophys Res* **87** (1982) 9171
7 G Haerendel *Report Max-Planck Inst. Phys. Astrophys Munich* (1973)
8 P K Chaturvedi and P K Kaw *J Geophys Res* **81** (1976) 3257
9 M K Hudson and C F Kennel *J Geophys Res* **80** (1975) 4581
10 A J Scannapieco and S L Ossakow *Geophys Res Lett* **3** (1976) 451
11 S T Zalesak and S L Ossakow *J Geophys Res* **85** (1980) 2131
12 B G Fejer and M C Kelley *Rev Geophys* **18** (1980) 401
13 S L Ossakow *J atmos Terr Phys* **43** (1981) 437
14 M C Kelley *The Earth's Ionosphere: Plasma Physics and Electrodynamics* Academic Press California (1989)
15 B V Krishna Murthy *Indian J Radio Space Phys* **22** (1993) 82
16 R Sekar, R Suhasini and R Raghavarao *J Geophys Res* **99** (1994) 2205
17 M C Kelley, M F Larson, C LaHoz and J P McClure *J Geophys Res* **86** (1981) 9087
18 D L Hysell, M C Kelley, W E Swartz and R F Woodman *J Geophys Res* **95** (1990) 17253
19 Chao-Song Huang, M C Kelley and D L Hysell *J Geophys Res* **98** (1993) 15631
20 Chao-Song Huang and M C Kelley *J Geophys Res* **101** (1996) 283
21 R Sekar, R Suhasini and R Raghavarao *Geophys Res Lett* **22** (1995) 885
22 Chao-Song Huang and M C Kelley *J Geophys Res* **101** (1996) 293
23 S Prakash *Indian J Radio & Space Phys* **25** (1996) 211
24 E Ott *J Geophys Res* **83** (1978) 2066
25 S L Ossakow and P K Chaturvedi *J Geophys Res* **83** (1978) 2085
26 M K Hudson *J Geophys Res* **83** (1978) 3189
27 D N Anderson and G Haerendel *J Geophys Res* **84** (1979) 4251
28 H Laakso, T L Aggson, R F Pfaff and W B Hanson *J Geophys Res* **99** (1994) 11507
29 P B Rao, A K Patra, T V Chandrasekhar Sarma, B V Krishna Murthy, K S V Subba Rao and S Hari *Radio Sci* **32** (1997) 1215
30 E Costa and M C Kelley *J Geophys Res* **83** (1978) 4359
31 D L Hysell, M C Kelley, W E Swartz, R F Pfaff and C M Swenson *J Geophys Res* **99** (1994) 8827
32 D L Hysell, C E Seyler and M C Kelley *J Geophys Res* **99** (1994) 8841
33 D L Hysell, M C Kelley, W E Swartz and D T Farley *J Geophys Res.* **99** (1994) 15065
34 E P Szuszczewicz, R T Tsunoda, R Narcisi and J C Holmes *Geophys Res Lett* **1** (1980) 537
35 R T Tsunoda, M J Baron, J Owen and D M Twole *Radio Sci* **14** (1979) 1111
36 D M Towle *Radio Sci* **15** (1980) 71
37 R T Tsunoda and D M Towle *Geophys Res Lett* **6** (1979) 873
38 S L Ossakow, S T Zalesak, B E McDonald and P K Chaturvedi *J Geophys Res* **84** (1979) 17
39 S T Zalesak and S L Ossakow *J Geophys Res* **87** (1982) 151
40 T L Aggson, N C Maynard, W B Hanson and J L Saba *J Geophys Res* **97** (1992) 2997
41 D L Hysell and D T Farley *J Geophys Res* **101** (1996) 5165
42 A K Patra, P B Rao, V K Anandan and A R Jain *J atmos Terr Phys* **59** (1997) 1633.
43 M C Kelley *J atmos Terr Phys* **47** (1985) 745
44 R Raghavarao, S P Gupta, R Sekar, R Narayanan, J N Desai, R Sridharan, V V Babu and V Sudhakar *J atmos Terr Phys* **49** (1987) 492
45 R Sekar and R Raghavarao *Geophys Res Lett* **22** (1995) 885
46 J Röttger *J atmos Terr Phys* **35** (1973) 1195
47 J Röttger *J atmos Terr Phys* **38** (1976) 97
48 J Röttger *J atmos Terr Phys* **40** (1978) 1103
49 J Klostermeyer *J Geophys Res* **83** (1978) 3753
50 S Prakash and R Pandey *J atmos Terr Phys* **47** (1985) 363
51 P K Chaturvedi and S L Ossakow *Geophys Res Lett* **4** (1977) 558
52 E Costa and M C Kelley *J Geophys Res* **83** (1978) 4365
53 J D Huba and S L Ossakow *J Geophys Res* **84** (1979) 6697
54 M Mendillo and A Tyler *J Geophys Res* **88** (1983) 5778
55 T L Aggson, H Laakso, N C Maynard and R F Pfaff *J Geophys Res* **101** (1996) 5152
56 R F Woodman *Proc COSPAR Colloq Low Latitude Ionospheric phys* (1994) 83
57 R Sekar, R Sridharan and R Raghavarao *J Geophys Res (submitted)* (1996)
58 S Chandrasekhar *Plasma Physics* University of Chicago Press (1960) 71